

## Article

# Synthesis and Laser-Related Spectroscopy of Er:Y<sub>2</sub>O<sub>3</sub> Optical Ceramics as a Gain Medium for In-Band-Pumped 1.6 μm Lasers

Konstantin N. Gorbachenya<sup>1</sup>, Anatol S. Yasukevich<sup>1</sup>, Viktor E. Kisel<sup>1</sup>, Kirill V. Lopukhin<sup>2</sup>, Vladimir V. Balashov<sup>2</sup>, Alexander V. Fedin<sup>3,4</sup>, Miron N. Gerke<sup>3</sup>, Elena A. Volkova<sup>5,\*</sup>, Vasiliy O. Yapaskurt<sup>5</sup>, Nikolay N. Kuzmin<sup>5,6,7</sup>, Dmitry A. Ksenofontov<sup>5</sup>, Dmitry V. Korost<sup>8</sup> and Nikolay V. Kuleshov<sup>1</sup>

<sup>1</sup> Center for Optical Materials and Technologies, Belarusian National Technical University, Nezalezhnasti Ave., 65, 220013 Minsk, Belarus; gorby@bntu.by (K.N.G.); anatol@bntu.by (A.S.Y.); vekisel@bntu.by (V.E.K.); nkuleshov@bntu.by (N.V.K.)

<sup>2</sup> Fryazino Branch of the Institution of Science, V.A. Kotelnikov Institute of Radio Engineering and Electronics, Russian Academy of Sciences, Vvedenskogo Sq. 1, 141190 Fryazino, Russia; xenon187@yandex.ru (K.V.L.); vla.dimir.ba@yandex.ru (V.V.B.)

<sup>3</sup> Department of Physics and Applied Mathematics, Vladimir State University, Gorky Str. 87, 600000 Vladimir, Russia; a\_fedin@list.ru (A.V.F.); miron\_gerke@mail.ru (M.N.G.)

<sup>4</sup> Kovrov State Technological Academy, Mayakovsky Str. 19, 601910 Kovrov, Russia

<sup>5</sup> Department of Crystallography and Crystal Chemistry, Faculty of Geology, Moscow State University, 119992 Moscow, Russia; vyapaskurt@mail.ru (V.O.Y.); kolyanfclm@mail.ru (N.N.K.); ksen53@gmail.com (D.A.K.)

<sup>6</sup> Institute of Spectroscopy, RAS, Fizicheskaya Str. 5, Troitsk, 108840 Moscow, Russia

<sup>7</sup> Moscow Institute of Physics and Technology, 9 Institutskiy Per., 141700 Dolgoprudny, Russia

<sup>8</sup> Department of Geology and Geochemistry of Fossil Fuels, Moscow State University, 119992 Moscow, Russia; dkorost@mail.ru

\* Correspondence: volkova@geol.msu.ru



**Citation:** Gorbachenya, K.N.;

Yasukevich, A.S.; Kisel, V.E.;

Lopukhin, K.V.; Balashov, V.V.; Fedin,

A.V.; Gerke, M.N.; Volkova, E.A.;

Yapaskurt, V.O.; Kuzmin, N.N.; et al.

Synthesis and Laser-Related

Spectroscopy of Er:Y<sub>2</sub>O<sub>3</sub> Optical

Ceramics as a Gain Medium for

In-Band-Pumped 1.6 μm Lasers.

*Crystals* **2022**, *12*, 519. <https://doi.org/10.3390/cryst12040519>

org/10.3390/cryst12040519

Academic Editor: Anna Paola

Caricato

Received: 14 March 2022

Accepted: 30 March 2022

Published: 8 April 2022

**Publisher's Note:** MDPI stays neutral with regard to jurisdictional claims in published maps and institutional affiliations.



**Copyright:** © 2022 by the authors. Licensee MDPI, Basel, Switzerland. This article is an open access article distributed under the terms and conditions of the Creative Commons Attribution (CC BY) license (<https://creativecommons.org/licenses/by/4.0/>).

**Abstract:** In this paper, Er:Y<sub>2</sub>O<sub>3</sub> optical ceramics were fabricated and details of the synthesis were presented. The spectral–luminescent properties of Er<sup>3+</sup>:Y<sub>2</sub>O<sub>3</sub> optical ceramics were investigated. The absorption and emission cross-section spectra were determined. The luminescence kinetics at near 1.6 μm was single exponential and the lifetime of erbium <sup>4</sup>I<sub>13/2</sub> energy level was determined. In the frame of the conventional Judd–Ofelt theory, the emission properties of the energy levels of erbium <sup>4</sup>I<sub>13/2</sub> and <sup>4</sup>I<sub>11/2</sub> involved in laser operation at near 1.6 μm were calculated. The gain coefficient curves for typical values of the relative population of the upper laser level <sup>4</sup>I<sub>13/2</sub> were presented. The composition and structure were studied using the SEM, XRD, FTIR spectroscopy, and X-ray computer tomography techniques.

**Keywords:** erbium; optical ceramics; sesquioxides; laser-related spectroscopy; structure

## 1. Introduction

Lasers emitting in the eye-safe spectral range of around 1.6 μm are of great interest for different applications in laser range finding, telecommunications, and optical location. Erbium solid-state lasers are widely used for this purpose because they are relatively simple, compact, and can operate in different lasing modes.

In-band pumping at near 1.5 μm (direct excitation of the Er<sup>3+</sup> ions to the upper laser energy level <sup>4</sup>I<sub>13/2</sub>) is a promising means of developing erbium lasers. One of the main advantages of such a pumping scheme is a significant reduction in the quantum defect and, consequently, thermal load. Moreover, in comparison with the Er–Yb sensitization pumping scheme (pumping to the <sup>2</sup>F<sub>5/2</sub> energy level of Yb<sup>3+</sup> ions and energy transfer to the <sup>4</sup>I<sub>11/2</sub> energy level of Er<sup>3+</sup> ions), losses owing to energy transfer and up-conversion from the intermediate <sup>4</sup>I<sub>11/2</sub> energy level can be avoided, resulting in a significantly higher lasing efficiency. In recent years, the increased research in this area has also been associated

with the appearance of the InGaAsP/InP laser diode, which emits near 1.5  $\mu\text{m}$  with good spectral and spatial properties [1].

Recently, different crystals doped with  $\text{Er}^{3+}$  ions have been considered as promising gain media for in-band-pumped erbium lasers emitting near 1.6  $\mu\text{m}$ : garnets [2–4], vanadates [5–8], tungstates [9,10], fluorides [11,12], and sesquioxides [13–15]. Sesquioxide crystals  $\text{Er}:\text{Re}_2\text{O}_3$  ( $\text{Re}=\text{Y}, \text{Sc}, \text{Lu}$ ) are isotropic crystals characterized by a high thermal conductivity ( $\sim 12.6 \text{ W/m} \times \text{K}$  for  $\text{Er}:\text{Lu}_2\text{O}_3$  crystal [13]) and intensive absorption peaks near 1.5  $\mu\text{m}$ , which coincide with the emission band of InGaAsP/InP laser diodes. Using  $\text{Er}$  (0.7 at.%) $:\text{Lu}_2\text{O}_3$ , the continuous-wave mode was demonstrated with a maximal output power of 1.26 W and slope efficiency of 32% at  $\sim 1.6 \mu\text{m}$  [14], while an up to 45% slope efficiency was realized for the  $\text{Er}:\text{Sc}_2\text{O}_3$  crystal [15].

However, the growth complexity is a major limitation for the application of sesquioxide crystals, mainly because of their high melting temperature, which is close to 2400  $^\circ\text{C}$ . One solution is to use optical ceramics based on these crystals. Modern technology makes it possible to fabricate samples with large dimensions and high optical qualities comparable with the corresponding crystals. At the same time, the price of fabricating optical ceramics is lower than the crystal growth, which ultimately leads to a decrease in laser production prices [16].

Recently, results concerning the synthesis and properties of  $\text{Er}:\text{Y}_2\text{O}_3$  ceramics fabricated using the HIP technique were reported in [17]. In this paper, we present the synthesis and structural characterization of sesquioxide ceramics and a detailed study of the laser-related spectroscopy of  $\text{Er}^{3+}:\text{Y}_2\text{O}_3$  optical ceramics as a gain medium for in-band-pumped 1.6  $\mu\text{m}$  lasers.

## 2. Experimental Details

### 2.1. Synthesis of $\text{Er}:\text{Y}_2\text{O}_3$ Optical Ceramics

High-purity  $\text{Y}_2\text{O}_3$  from ‘Nevatorg’, St. Petersburg, Russia,  $\text{Er}_2\text{O}_3$  (0.25 and 0.5 mol.%) produced by Lanhit, Moscow, Russia were used as the starting materials.  $\text{MgO}$  (0.01 mol.%),  $\text{ZrO}_2$  (1.5 mol.%), and  $\text{La}_2\text{O}_3$  (0.5 mol.%) were used as sintering aids. Before mixing, all initial powders were annealed in air at 1050  $^\circ\text{C}$  for 5 h. The preliminary annealing of the initial powder allows for the better control of the viscosity of the slurry during milling.

The powders were mixed and ground in a planetary mill using anhydrous isopropyl alcohol as a medium with the addition of 1 wt.% MFO (Menhaden Fish Oil, The Tape Casting Warehouse Inc., Morrisville, PA, USA) as a dispersant. Milling was carried out in two stages in Nylon-6 containers using high-purity zirconium balls. In the first stage, the powder was milled at a volume ratio of 6.5:1 (alcohol/powder) for 10 h. The containers were then removed from the mill, the alcohol ratio was increased to 6.8–7.0, and the powder was milled for another 10 h. The addition of alcohol in the middle of the milling cycle kept the viscosity in the optimal range. To the best of our knowledge, this double-stage milling process has not been used by other research groups. The powder mixture was then dried at 60  $^\circ\text{C}$  for 3 days, annealed in air at 600  $^\circ\text{C}$  for 7 h to remove the dispersant, and sieved through a 200-mesh sieve. After sieving, the powder was annealed again in the air at 900  $^\circ\text{C}$  to remove the remaining organic impurities. The post-milling annealing temperature was kept lower than the temperature of the first annealing so that the powder particles would not fuse together before pressing.

Compacts 35 mm in diameter were pressed from the prepared powder. Uniaxial pressing was carried out in a metal mold with one movable punch. Each compact was pressed in two stages. In the first stage, 7 g of powder was poured into the mold, the upper punch was inserted, and a pressure of 10 MPa was applied. Next, the pressure was released, the mold was taken out of the press, and the upper punch was turned by hand (to separate it from the compact) and carefully removed. Then, another 4 g of powder was poured into the mold and a pressure of 40 MPa was applied and maintained for 3 min (holding is necessary to prevent the delamination of the two parts). In uniaxial pressing, the inhomogeneity of the compact increases as its thickness increases, while pressing in

two stages with the addition of powder allows the powder particles to be compacted more uniformly throughout the thickness of the compact.

After uniaxial pressing, the compacts were annealed in air at 900 °C and then subjected to cold isostatic pressing (CIP) at a maximum pressure of 250 MPa. The pressure profile used during the CIP cycle has not been previously reported:

- (1) Increase pressure up to 180 MPa in 5 min, hold for 2 min.
- (2) Drop to 125 MPa in 2 min, hold for 2 min.
- (3) Increase to 215 MPa in 2 min, hold for 2 min.
- (4) Drop to 165 MPa in 2 min, hold for 2 min.
- (5) Increase to maximum 250 MPa in 2 min, hold for 5 min.
- (6) Gradual pressure release from 250 MPa to 0 MPa in 15 min.

As the pressure increases, the powder particles in the compact move relative to each other. This movement is both translational and rotational. The pressure protocol described provides the particles more opportunities to move and therefore fill more voids in the compact. After CIP, the samples were annealed in air at 1100 °C for 8 h to remove the remaining volatile impurities. The compacts were then sintered in a vacuum furnace with a tungsten heating element at a temperature and holding time of 1875 °C and 20 h, respectively. A special aspect of our sintering method is that the rate of temperature increase was slowed to 0.04 degrees per minute in the range 1780–1840 °C. The resulting ceramic samples were first annealed in air at 1100 °C for 30 h and then at 1300 °C for 25 h to remove the oxygen vacancies formed during vacuum sintering. Subsequently, the samples were ground and polished.

## 2.2. Experimental Techniques for Investigation of the Composition, Structure, and Spectroscopic Properties of $\text{Er}^{3+}:\text{Y}_2\text{O}_3$

The microstructure and elemental analysis were performed by the analytical scanning electron microscopy (SEM) technique using a JSM-IT500 microscope, JEOL Ltd., Japan, equipped with the energy-dispersive X-ray (EDX) detector X-Max-50, Oxford Instruments Ltd., GB (purchased under the “Program of MSU Development”), in the Laboratory of Local Methods for the Study of Matter (Faculty of Geology, MSU).

Powder X-ray diffraction (PXRD) studies were carried out on a Rigaku MiniFlex-600 powder diffractometer, Rigaku Corp., Japan. PXRD datasets were collected in continuous mode at room temperature using  $\text{CuK}\alpha$  radiation ( $\lambda = 1.54056 \text{ \AA}$ ) in the range of  $2\theta = 3\text{--}70^\circ$ , step size of  $0.05^\circ$ , and scan speed of  $3^\circ$  per minute. Phase identification was performed using a crystallographic open database (COD). The unit cell parameters were calculated using the DICVOL06 program implemented in the FullProf program suite [18].

A 3D structure of  $\text{Er}:\text{Y}_2\text{O}_3$  ceramics was studied via the X-ray computer tomography (XRCT) technique using Phoenix v|tome|x M tomography system, General Electric, Wunstorf, Germany, equipped with scatter X-ray correction technology. The following settings were applied: resolution 4.5  $\mu\text{m}$ , voltage 160 kV, current 120 mA, and timing 750 ms.

The absorption spectra of  $\text{Er}$  (0.25 and 0.5 mol.%) $:\text{Y}_2\text{O}_3$  in the far- and mid-IR regions were recorded using a Bruker IFS 125HR Fourier spectrometer. For measurements in the  $100\text{--}500 \text{ cm}^{-1}$  range, a polycrystalline  $\text{Er}:\text{Y}_2\text{O}_3$  powder weighing 2 mg was ground in an agate mortar with 50 mg of polyethylene; for measurements in the  $400\text{--}700 \text{ cm}^{-1}$  range, the sample was prepared in a similar way from 5 mg of  $\text{Er}:\text{Y}_2\text{O}_3$  and 200 mg of KBr. The mixtures were then pressed into tablets. Absorption spectra in the far-IR range were obtained at room temperature with a resolution of  $4 \text{ cm}^{-1}$  and in the mid-IR range with a resolution of  $2 \text{ cm}^{-1}$ .

The absorption spectra in the spectral range 350–1650 nm of  $\text{Er}^{3+}:\text{Y}_2\text{O}_3$  transparent ceramics sample at room temperature were registered by a Varian CARY 5000 spectrophotometer and the SBW was 0.5 nm.

The absorption coefficients  $k_{abs}(\lambda)$  and the absorption cross-sections  $\sigma_{abs}(\lambda)$  were calculated by:

$$k_{abs}(\lambda) = \frac{D(\lambda) \ln(10)}{l} , \sigma_{abs}(\lambda) = \frac{k_{abs}(\lambda)}{N_{Er}} ,$$

where  $l$  is the samples' thickness and  $N_{Er}$  is the erbium concentration.

The luminescence spectrum was recorded in the 1400–1700 nm spectral range by exciting the crystals with the emission of the laser diode at 960 nm. The  $Er^{3+}$  luminescence radiation was dispersed with the MDR-23 monochromator (LOMO, Russia) and detected with the PbS photoresistor supplied with a preamplifier connected to the Stanford Research Lock-In Amplifier SP830 (Stanford Research Systems, Sunnyvale, CA, USA).

The lifetime measurements were performed using the optical parametric oscillator based on a  $\beta$ - $Ba_2B_2O_4$  crystal and pumped by the third harmonic of the Q-switched Nd:YAG laser. The fluorescence from the sample was collected on the entrance slit of the monochromator MDR-12 and registered by the InGaAs photodiode with a preamplifier coupled with a 500 MHz digital oscilloscope.

In the frame of conventional Judd–Ofelt (J–O) theory, the strengths of absorption and emission transitions were calculated.

The stimulated emission cross-section spectrum in the spectral range 1420–1700 nm was calculated using the two techniques, the modified reciprocity method (MRM) and the Füchtbauer–Ladenburgh equation (FLE) [19], using the radiative lifetime  $\tau_{rad}$  of  $^4I_{13/2}$  energy level of  $Er^{3+}$  ions obtained from the J–O theory.

$$\sigma_{em}(\lambda) = \frac{\exp(-hc/(kT\lambda))}{8\pi n^2 \tau_{rad} c \int \lambda^{-4} \sigma_{abs}(\lambda) \exp(-hc/(kT\lambda)) d\lambda} \sigma_{abs}(\lambda) \quad (1)$$

$$\sigma_{em}(\lambda) = \frac{\lambda^5}{8\pi n^2 \tau_{rad} c} \frac{W_{em}(\lambda)}{\int \lambda W_{em}(\lambda) d\lambda} \quad (2)$$

Here,  $W_{em}(\lambda)$  is the spectral density of luminescence power;  $c$  is the speed of light;  $h$  and  $k$  are Planck's and Boltzmann's constants, respectively;  $T$  is the host ceramic's temperature; and  $n$  is the refractive index of the ceramics.

The gain spectra  $g(\lambda)$  were calculated for different inversion parameters  $\beta$  using the following equation:

$$g(\lambda) = N_{Er}(\sigma_1(\lambda)\beta - \sigma_{abs}(\lambda)), \quad (3)$$

where  $\sigma_1(\lambda) = \sigma_{abs}(\lambda) + \sigma_{em}(\lambda)$  and  $\beta = N(^4I_{13/2})/N_{Er}$ .

### 3. Results and Discussion

#### 3.1. Synthesis, Structure, and Composition

$Er$  (0.25 mol.%): $Y_2O_3$  and  $Er$  (0.5 mol.%): $Y_2O_3$  samples of transparent ceramics with a high optical quality (transmission coefficient more than 99% at 600 nm), diameter > 20 mm, and thickness > 3 mm were produced. The photo of the  $Er^{3+}$ : $Y_2O_3$  optical ceramics used for spectroscopy investigation is presented in Figure 1.

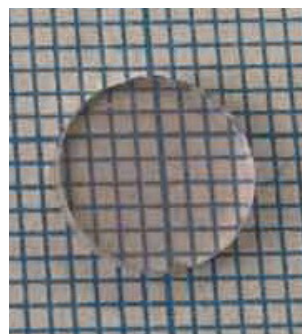


**Figure 1.**  $Er^{3+}$ : $Y_2O_3$  optical ceramics.

The phase purity and structure of Er (0.25 and 0.5 mol.%):Y<sub>2</sub>O<sub>3</sub> ceramics were confirmed using the XRD method (Figure 2). PXRD patterns fit well with the theoretical ones calculated from the *cif*-file for Y<sub>2</sub>O<sub>3</sub> (COD ID 1009015). Er (0.25 and 0.5 mol.%):Y<sub>2</sub>O<sub>3</sub> are cubic with sp.gr. *Ia* $\bar{3}$ . The lattice constants for both samples are similar:  $a = 10.5974(2)$  Å for Er (0.25 mol.%):Y<sub>2</sub>O<sub>3</sub> and  $a = 10.5959(4)$  Å for Er (0.5 at.%):Y<sub>2</sub>O<sub>3</sub>. No traces of any impurity or glassy phases were found.

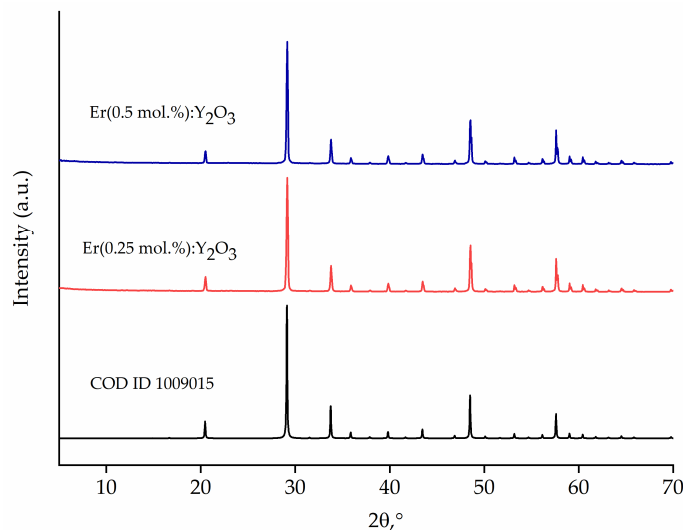


**Figure 2.** PXRD patterns of Er (0.25 and 0.5 mol.%):Y<sub>2</sub>O<sub>3</sub> ceramics samples compared with the theoretical pattern for Y<sub>2</sub>O<sub>3</sub> (COD ID 1009015).

Phonon spectra were examined to confirm the structure of the Er<sup>3+</sup>:Y<sub>2</sub>O<sub>3</sub> ceramics. This method was used because the high sensitivity of FTIR spectroscopy with known IR spectra allows for the easy identification of associated or intermediate phases even in low concentrations. Figure 3 demonstrates the absorption spectrum of Er (0.5 mol.%):Y<sub>2</sub>O<sub>3</sub> in the far- and mid-IR ranges at room temperature. A similar absorption spectrum was observed for an Er (0.25 mol.%):Y<sub>2</sub>O<sub>3</sub> sample. We observed 12 strong phonons  $F_u$  from the phonon spectra. These correspond to the earlier results from Ref. [20], where 16 infrared active phonons were computed from the group theoretical analysis. The missing four phonons were probably not resolved in the spectra due to the fact that there were phonons with similar frequencies in this crystal.

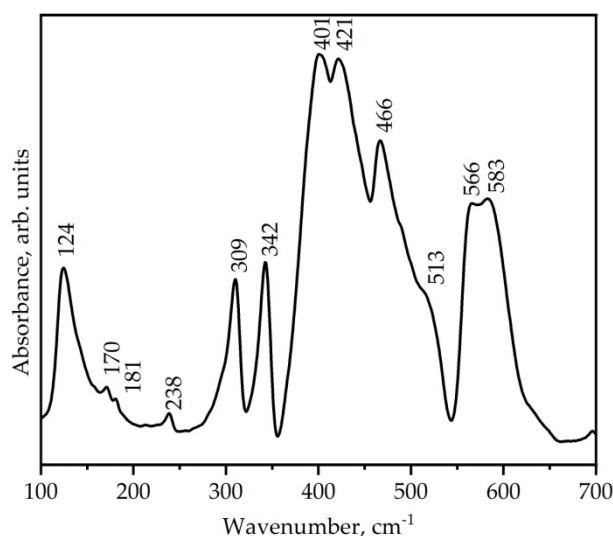


**Figure 3.** IR absorption spectrum of Er (0.5 mol.%):Y<sub>2</sub>O<sub>3</sub>.

XRCT scanning demonstrates that the synthesized ceramics specimens were characterized by homogeneous microstructures without any associated phases (Figure 4).

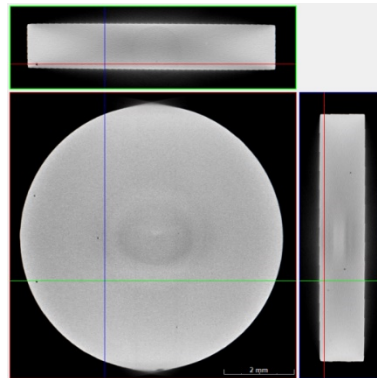


**Figure 4.** Three-dimensional image of Er (0.5 mol.):Y<sub>2</sub>O<sub>3</sub> ceramics.

Figure 5 shows the SEM micrograph of the Er (0.5 mol.):Y<sub>2</sub>O<sub>3</sub> sample. The ceramics materials were characterized by several residual pores, and mainly flat grain boundaries were observed. There were no apparent differences in the porosity and grain size for the two samples as a function of the dopant concentration due to the similar ionic radii of Er<sup>3+</sup> and Y<sup>3+</sup> cations and minor differences in the Er<sup>3+</sup> content. According to the EDX analysis, the average content of Er<sup>3+</sup> almost corresponded to that in the initial load.

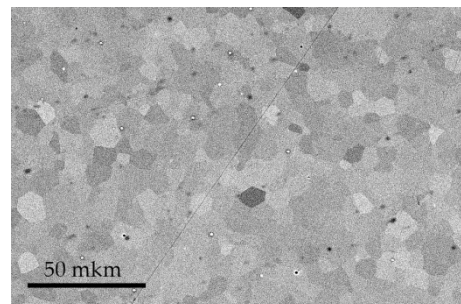


**Figure 5.** BSE image of Er (0.5 mol.):Y<sub>2</sub>O<sub>3</sub> ceramics providing the orientation contrast of grains.

### 3.2. Absorption Spectra and Judd–Ofelt Calculations

The absorption spectra from the ground state  $^4I_{15/2}$  to upper lying excited states are shown in Figure 6. The assignment of the spectral lines was made on the basis of Refs. [21,22].

The spectral lines in the regions of 350–370 nm (Figure 6a) and 440–465 nm (Figure 6b) corresponding to the transitions  $^4I_{15/2} \rightarrow ^2K_{15/2}$ ,  $^4I_{15/2} \rightarrow ^4G_{9/2}$ ,  $^4I_{15/2} \rightarrow ^2G(1)_{7/2}$  and transitions  $^4I_{15/2} \rightarrow ^4F_{5/2}$ ,  $^4I_{15/2} \rightarrow ^4F_{3/2}$ , respectively, overlap substantially, so they will be considered in the J–O calculations as some effective spectral lines with overall oscillator strengths.

The J–O theory considers electronic transitions between the energy levels of trivalent lanthanides, caused mainly by electric and magnetic dipoles, and allows for the calculation of the radiative properties of media doped with rare-earth ions. The fundamentals and numerous applications have been widely discussed in the literature—e.g., see Refs. [23–25].

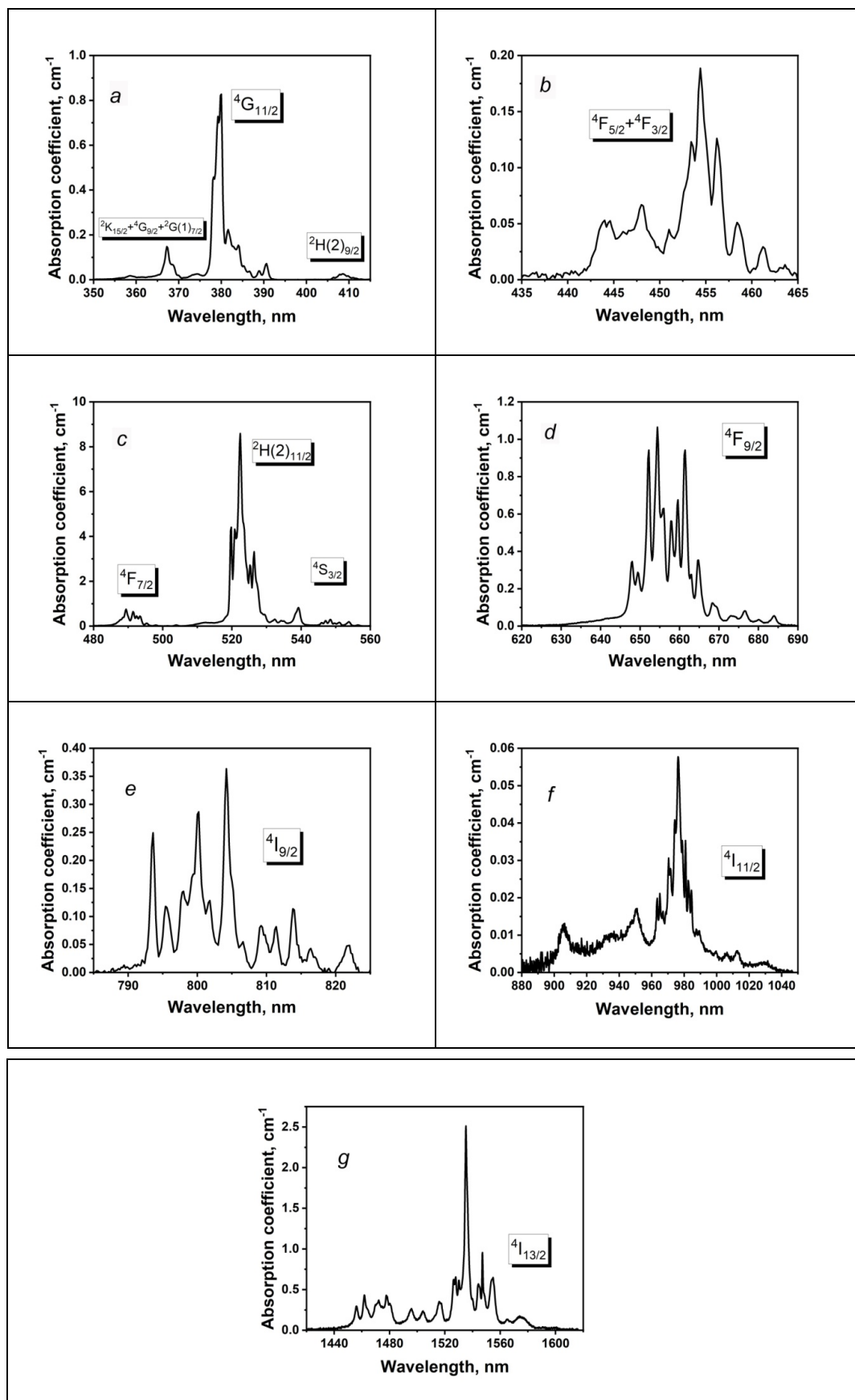


**Figure 6.** The absorption coefficients spectra of Er<sup>3+</sup>:Y<sub>2</sub>O<sub>3</sub> optical ceramics: (a) in the spectral range of 350–410 nm; (b) in the spectral range of 435–465 nm; (c) in the spectral range of 480–560 nm; (d) in the spectral range of 620–690 nm; (e) in the spectral range of 780–830 nm; (f) in the spectral range of 880–1050 nm; (g) in the spectral range of 1430–1650 nm.

The selection rules for the magnetic-dipole transition in the Russell–Saunders approximation are as follows [26]:

$$J' = J, J + 1, J - 1 \quad L' = L \quad S' = S$$

In our case, the transitions in absorption  ${}^4I_{15/2} \rightarrow {}^4I_{13/2}$  and emission  ${}^4I_{11/2} \rightarrow {}^4I_{13/2}$  satisfy these selection rules. The magnetic-dipole oscillator strengths of these transitions may be calculated directly by:

$$f_{calc}^{md} = \frac{8\pi^2 mc}{3he^2} \frac{1}{\bar{\lambda}} \frac{n}{2J+1} S^{md}$$

Here,  $m$  is the electron mass,  $\bar{\lambda}$  is the mean wavelength of the  $JJ'$  transition,  $J$  is the quantum number of the total angular momentum for the initial state,  $S^{md}$  is the magnetic-dipole line strength [26]:

$$S_{calc}^{md} = \left( \frac{e}{2mc} \right)^2 |\langle [SL]J || \hat{L} + 2\hat{S} || [S'L']J' \rangle|^2$$

which is calculated over the set of eigenvectors  $|[SL]J\rangle = \sum_{S,L} C(S,L) |SLJ\rangle$  (see Table 1).

**Table 1.** The wavefunctions of the  $|[4I]15/2\rangle$ ,  $|[4I]13/2\rangle$ , and  $|[4I]11/2\rangle$  eigenvectors.

	4G	4I	2H1	2H2	2I	2K	2L
$ [4I]15/2\rangle$	0.0000	0.9852	0.0000	0.0000	0.0000	−0.1703	−0.0174
$ [4I]13/2\rangle$	0.0000	0.9955	0.0000	0.0000	0.0317	−0.0894	0.0000
$ [4I]11/2\rangle$	−0.1146	−0.9067	0.1096	−0.3858	−0.0631	0.0000	0.0000

The experimental oscillator strength:

$$f_{exp} = \frac{mc}{\pi e^2 N_{Er} \bar{\lambda}^2} \int k_{abs}(\lambda) d\lambda$$

which includes the electric dipole as well as magnetic dipole mechanisms. The experimental values of the electric-dipole oscillator strengths are calculated as:

$$f_{exp}^{ed} = f_{exp} - f_{calc}^{md}$$

and the experimental electric dipole line strengths are determined as:

$$S_{exp}^{ed} = \frac{3h(2J+1)\bar{\lambda}}{8\pi^2 mc} \frac{9n}{(n^2+2)^2} f_{exp}^{ed}$$

According to the J–O theory [23–25], the line strength of the electric dipole transition between manifolds with quantum numbers  $J$  and  $J'$  can be expressed as:

$$S_{calc}^{ed} = \sum_{\lambda=2,4,6} \Omega_{\lambda} |\langle [SL]J || U^{(\lambda)} || [S'L']J' \rangle|^2$$

where  $\langle ||U^t|| \rangle$  are reduced-matrix elements of the unit tensor operator  $U^{(t)}$  of rank  $t$  and the  $\Omega_{\lambda}$  are empirical parameters. The parameters  $\Omega_{\lambda}$  obtained by the least-square fitting of the calculated values  $S_{calc}^{ed}$  to the experimental ones  $S_{exp}^{ed}$  are presented in Table 2. One can see that they are in good agreement with the parameters reported in Ref. [17] for  $\text{Er}^{3+}:\text{Y}_2\text{O}_3$  ceramics. It is noteworthy that for both ceramics' materials, the intensity parameter  $\Omega_2$  is larger than for the  $\text{Er}^{3+}$ -doped single crystal  $\text{Y}_2\text{O}_3$  [21]. This evidences the fact that the local symmetry of  $\text{Er}^{3+}$  ions in the crystalline media is higher than that in the ceramic.

**Table 2.** The J–O intensity parameters  $\Omega_{2,4,6}$  of  $\text{Er}^{3+}$ .

$\Omega_2 \times 10^{-20}, \text{cm}^2$	$\Omega_4 \times 10^{-20}, \text{cm}^2$	$\Omega_6 \times 10^{-20}, \text{cm}^2$	Reference
6.068	1.223	0.790	This work
4.57	1.76	0.85	[17]
3.611	1.347	1.27	[21]

The experimental and calculated electric dipole absorption oscillator strengths are presented in Table 3.

**Table 3.** Experimental ( $f_{exp}^{ed}$ ) and calculated ( $f_{calc}^{ed}$ ) oscillator strengths of  $\text{Er}^{3+}$  in  $\text{Y}_2\text{O}_3$ .

Excited Energy Levels	$\lambda, \text{nm}$	$f_{exp}^{ed} \times 10^6$	$f_{calc}^{ed} \times 10^6$
${}^2\text{K}_{15/2} + {}^4\text{G}_{9/2} + {}^2\text{G}(1)_{7/2}$	366	3.08	2.40
${}^4\text{G}_{11/2}$	381	20.82	20.64
${}^2\text{H}(2)_{9/2}$	409	0.65	0.61
${}^4\text{F}_{5/2} + {}^4\text{F}_{3/2}$	452	0.45	0.76
${}^4\text{F}_{7/2}$	491	1.19	1.72
${}^2\text{H}(2)_{11/2}$	524	11.44	11.66
${}^4\text{S}_{3/2}$	550	0.42	0.40
${}^4\text{F}_{9/2}$	657	1.91	1.93
${}^4\text{I}_{9/2}$	803	0.30	0.34
${}^4\text{I}_{11/2}$	961	1.11	0.63
${}^4\text{I}_{13/2}$	1521	1.12	1.14
RMS deviation		$0.38 \times 10^{-6}$	

The transition probability  $A(JJ')$  of any excited state should include both the electric-dipole and magnetic-dipole contributions:

$$A(JJ') = \frac{64\pi^4 e^2}{3h(2J+1)\lambda^3} \left[ \frac{n(n^2+2)^2}{9} S_{calc}^{ed} + n^3 S_{calc}^{md} \right]$$

$J$  and  $J'$  are the total angular momentum of the upper and lower states, respectively. The calculated luminescence branching ratio for  $J \rightarrow J'$  transition is defined as:

$$\beta_{JJ'} = \frac{A(JJ')}{\sum_{J'} A(JJ')}$$

The radiative lifetime is defined as:

$$\tau_{rad} = \frac{1}{\sum_{J'} A(JJ')}$$

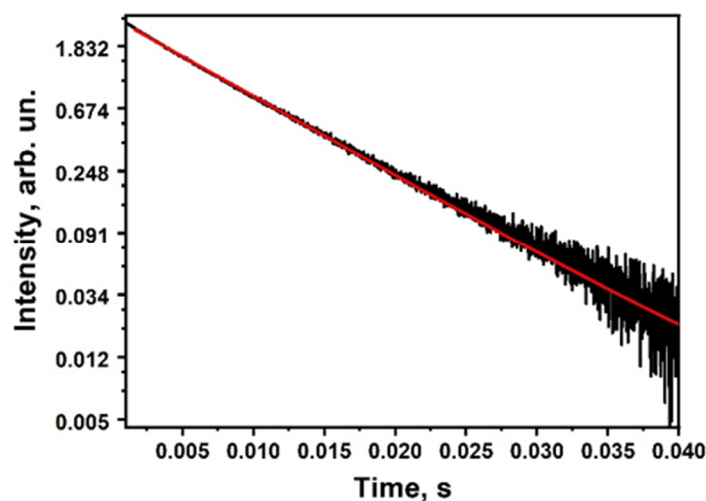
The radiative lifetimes,  $\tau_{rad}$ , and the luminescence branching coefficients,  $\beta_{JJ'}$ , obtained by the J–O calculations are given in Table 4.

It should be noted that the magnitudes of  $\beta_{JJ'}$  for the  ${}^4\text{I}_{11/2} \rightarrow {}^4\text{I}_{13/2}$  transition obtained in our work and in [17,21] are in moderate agreement, but the radiative times differ significantly. Some further studies of the issue could potentially be necessary to clarify these discrepancies.

The decay curve of 1.6  $\mu\text{m}$  emission was single exponential and the luminescence decay time  $\tau$  of the  ${}^4\text{I}_{13/2}$  level was measured to be 7.5  $\pm$  0.5 ms. (Figure 7). The measured lifetime was close to the radiative lifetime calculated from the J–O analysis. Thus, the luminescence quantum yield was estimated to be close to 1.

**Table 4.** Calculated  $\beta_{JJ'}$ , and  $\tau_{rad}$ .

Transition	$\beta_{JJ'}$ (%)	$\tau_{rad}$ (ms)	
${}^4I_{11/2} \rightarrow {}^4I_{13/2}$	12	4.06	This work
	16	7.99	[17]
	17.1	3.43	[21]
${}^4I_{15/2}$	88		This work
	84		[17]
	82.9		[21]
${}^4I_{13/2} \rightarrow {}^4I_{15/2}$	100	7.38	This work
	100	7.8	[17]
	100	4.88	[21]

**Figure 7.** The luminescence kinetics near 1.6  $\mu\text{m}$ .

The absorption cross-section spectrum of the  $\text{Er}^{3+}:\text{Y}_2\text{O}_3$  optical ceramics in the spectral range of 1420–1700 nm is presented in Figure 8 along with the stimulated emission cross-section spectra (SECS), calculated using the MRM (1) and FLE (2). The maximal absorption cross-section of  $1.28 \times 10^{-20} \text{ cm}^2$  was observed at 1536 nm. This wavelength is close to the spectral locations of emission spectra of the commercially available InGaAsP/InP laser diodes, which gives us the opportunity to consider the  $\text{Er}^{3+}:\text{Y}_2\text{O}_3$  optical ceramics as a promising laser medium under in-band pumping. The presence of two lines in the absorption spectrum at 1640 nm and 1660 nm is noteworthy, as they were first reported in [17]. These lines are also evident in the SECS spectra, which gives a possibility to expand the gain curve to the region 1640–1660 nm.

The highest magnitude of the SECS of  $1.16 \times 10^{-20} \text{ cm}^2$  is located at 1535 nm (MRM). The same peak magnitude of the SECS at 1535 nm calculated by the FLE is much lower, which we attribute to the reabsorption of the luminescence emission in the sample. In the region of 1640–1660 nm, the highest magnitudes of the SECS are as follows:  $0.84 \times 10^{-21} \text{ cm}^2$  (1641 nm) and  $0.63 \times 10^{-21} \text{ cm}^2$  (1663 nm), as calculated by the MRM and  $1.1 \times 10^{-21} \text{ cm}^2$  (1641 nm), and  $0.94 \times 10^{-21} \text{ cm}^2$  (1663 nm), as calculated by the FLE. One can see that the results obtained by both methods are in good agreement.

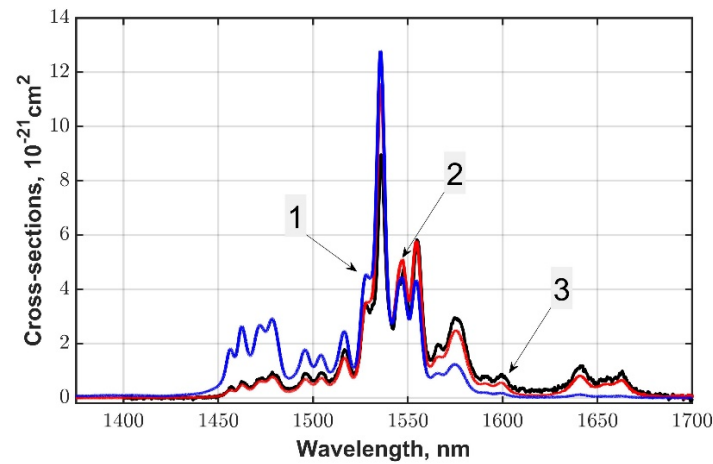


**Figure 8.** Absorption (1, blue) and emission (2, red; 3, black) cross-section spectra of  $\text{Er}^{3+}:\text{Y}_2\text{O}_3$  optical ceramics. 2—MRM; 3—FLE.

The gain spectra of  $\text{Er}:\text{Y}_2\text{O}_3$  optical ceramics for different inversion parameters  $\beta$  are presented in Figure 9. By using the laser setup described in detail in [6,9,11], the laser operation at 1575 nm, 1641 nm, and 1663 nm can be obtained.

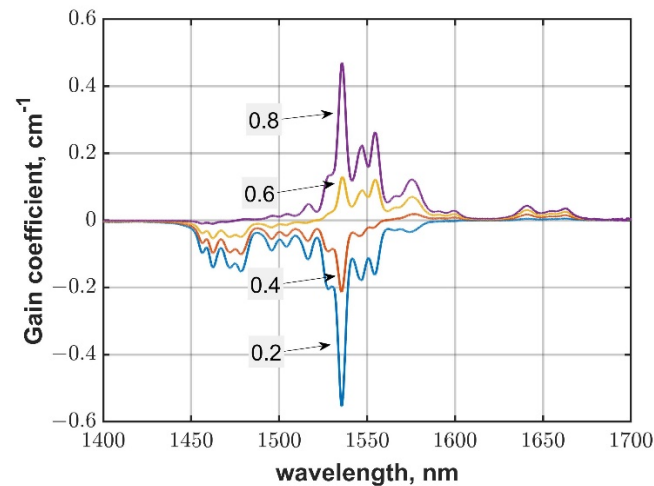


**Figure 9.** Gain spectra of  $\text{Er}^{3+}:\text{Y}_2\text{O}_3$  optical ceramics for inversion parameters.  $\beta = 0.2\text{--}0.8$ .

It is interesting to estimate the minimal absorbed pump power  $P_{min}^{abs}$  for different laser wavelengths  $\lambda_l$  of 1575 nm, 1641 nm, and 1663 nm when the gain and absorption coefficients equal zero for the case zero cavity losses. It can be easily derived from (3) that the minimal inversion parameter  $\beta_{min}$  at a certain wavelength  $\lambda$  is as follows:

$$\beta_{min} = \sigma_{abs} / \sigma_l$$

and:

$$P_{min}^{abs} = \frac{V_p h \nu_p N_{Er}}{\tau} \beta_{min}$$

Here, typical parameters for resonance pump conditions of erbium-doped laser materials were chosen [6,11].  $V_p = \pi \omega_p^2 l_a / 2$  is the pump volume,  $\omega_p$  is the Gaussian radius of the pump beam ( $\sim 25 \mu\text{m}$ ),  $l_a$  is the length of the active element ( $\sim 10 \text{mm}$ ), and  $h \nu_p$  is the energy quant of the pump radiation. We consider a pump source at 1531 nm—CW Er,Yb:GdAB laser [27]. The spectroscopic parameters were taken from our spectroscopic data (see Figure 9). In Table 5, the results of  $P_{min}^{abs}$  calculations are given.

**Table 5.** Calculated  $P_{min}^{abs}$ , and  $\beta_{min}$  for different laser wavelengths.

$\lambda_l$ , nm	$\beta_{min}$	$P_{min}^{abs}$ , mW
1576	0.3	2.3
1641	0.1	0.76
1663	0.07	0.53

These results are in good agreement with the same values estimated by us during the laser experiments for vanadates, fluorides, and tungstates crystals in [6,9,11].

#### 4. Conclusions

The Er:Y<sub>2</sub>O<sub>3</sub> optical ceramics were fabricated. New additives (namely, 0.5 mol.% La<sub>2</sub>O<sub>3</sub>, 1.5 mol.% ZrO<sub>2</sub>, and 0.01 mol.% MgO) were used in the sintering process to reduce the average ceramic grain size and improve its optical properties. In addition, a specific heat treatment profile was used during the preparation process. Er:Y<sub>2</sub>O<sub>3</sub> specimens were characterized by PXRD, SEM- and FTIR spectroscopy, and XRCT techniques. A detailed investigation on the spectral-luminescent properties of the Er:Y<sub>2</sub>O<sub>3</sub> optical ceramics was performed. The obtained spectroscopic characteristics indicate the promise of the use of Er:Y<sub>2</sub>O<sub>3</sub> optical ceramics as an active medium for eye-safe in-band-pumped lasers emitting near 1.6 μm for application in laser rangefinder, LIBS, and LIDAR systems.

**Author Contributions:** Writing—original draft preparation, K.N.G., K.V.L., V.V.B., A.V.F., M.N.G., E.A.V.; resources, K.V.L., V.V.B., E.A.V., A.V.F., M.N.G., N.V.K.; investigation, K.V.L., V.V.B., V.E.K., N.V.K., A.V.F., M.N.G., E.A.V., V.O.Y., N.N.K., D.A.K., D.V.K.; Formal analysis and investigation A.S.Y. All authors have read and agreed to the published version of the manuscript.

**Funding:** This research was partially supported by BRFFR F20R-035.

**Conflicts of Interest:** The authors declare no conflict of interest.

#### References

- Dubinskii, M.; Fromzel, V.; Ter-Gabrielyan, N.; Serrano, M.D.; Lahera, D.E.; Cascales, C.; Zaldo, C. Spectroscopic characterization and laser performance of resonantly diode-pumped Er<sup>3+</sup>-doped disordered NaY(WO<sub>4</sub>)<sub>2</sub>. *Opt. Lett.* **2011**, *36*, 3263–3265. [CrossRef]
- Shen, D.Y.; Sahu, J.K.; Clarkson, W.A. Highly efficient in-band pumped Er:YAG laser with 60 W of output at 1645 nm. *Opt. Lett.* **2006**, *31*, 754–756. [CrossRef]
- Ter-Gabrielyan, N.; Fromzel, V.; Mu, X.; Meissner, H.; Dubinskii, M. Resonantly pumped single-mode channel waveguide Er:YAG laser with nearly quantum defect limited efficiency. *Opt. Lett.* **2013**, *38*, 2431–2433. [CrossRef]
- Garbuzov, D.; Kudryashov, I.; Dubinskii, M. Resonantly diode laser pumped 1.6-μm-erbium-doped yttrium aluminum garnet solid-state laser. *Appl. Phys. Lett.* **2005**, *87*, 131115–131118. [CrossRef]
- Ter-Gabrielyan, N.; Fromzel, V.; Lukasiewicz, T.; Ryba-Romanowski, W.; Dubinskii, M. Nearly quantum-defect-limited efficiency, resonantly pumped, Er<sup>3+</sup>:YVO<sub>4</sub> laser at 1593.5 nm. *Opt. Lett.* **2011**, *36*, 1218–1220. [CrossRef] [PubMed]
- Gorbachenya, K.N.; Kisel, V.E.; Yasukevich, A.S.; Matrosov, V.N.; Tolstik, N.A.; Kuleshov, N.V. CW Er:YVO<sub>4</sub> laser with resonant pumping. *J. Appl. Spectrosc.* **2015**, *82*, 208–212. [CrossRef]
- Ter-Gabrielyan, N.; Fromzel, V.; Ryba-Romanowski, W.; Lukasiewicz, T.; Dubinskii, M. Spectroscopic properties and laser performance of resonantly-pumped cryo-cooled Er<sup>3+</sup>:GdVO<sub>4</sub>. *Opt. Express* **2012**, *20*, 6080–6084. [CrossRef]
- Ter-Gabrielyan, N.; Fromzel, V.; Yan, Z.; Han, X.; Zhang, H.; Wang, J.; Dubinskii, M. Highly efficient resonantly pumped Er<sup>3+</sup>:LuVO<sub>4</sub> laser. *Opt. Mater. Express* **2014**, *4*, 1355–1360. [CrossRef]
- Gorbachenya, K.N.; Kisel, V.E.; Yasukevich, A.S.; Pavlyuk, A.A.; Kuleshov, N.V. In-band pumped room-temperature Er:KY(WO<sub>4</sub>)<sub>2</sub> laser emitting near 1.6 μm. *Laser Phys.* **2013**, *23*, 125005. [CrossRef]
- Serrano, M.D.; Cascales, C.; Han, X.; Zaldo, C.; Jezowski, A.; Stachowiak, P.; Ter-Gabrielyan, N.; Fromzel, V.; Dubinskii, M. Thermal Characterization. Crystal field analysis and in-band pumped laser performance of Er-doped NaY(WO<sub>4</sub>)<sub>2</sub> disordered laser crystals. *PLoS ONE* **2013**, *8*, 59381–59383. [CrossRef]
- Gorbachenya, K.N.; Kurilchik, S.V.; Kisel, V.E.; Yasukevich, A.S.; Kuleshov, N.V.; Nizamutdinov, A.S.; Korableva, S.L.; Semashko, V.V. Lasing in resonantly pumped Er:LiYF<sub>4</sub> and Er:LiLuF<sub>4</sub> crystals. *Quantum Electron* **2016**, *46*, 95–99. [CrossRef]
- Moglia, F.; Brandt, C.; Huber, G. Inband-pumped Er<sup>3+</sup>: LiLuF<sub>4</sub> laser emitting in the 1.6 μm spectral range. In Proceedings of the Advanced Solid-State Photonics: Conference Paper, San-Diego, CA, USA, 29 January–1 February 2012; Optical Society of America: San-Diego, CA, USA, 2009. AM4A.22.

13. Merkle, L.D.; Ter-Gabrielyan, N.; Kacik, N.J.; Sanamyan, T.; Zhang, H.; Yu, H.; Wang, J.; Dubinskii, M. Er:Lu<sub>2</sub>O<sub>3</sub>—Laser-related spectroscopy. *Opt. Mater. Express* **2013**, *3*, 1992–2002. [[CrossRef](#)]
14. Brandt, C.; Tolstik, N.A.; Kuleshov, N.V.; Petermann, K.; Huber, G. In-band pumped Er:Lu<sub>2</sub>O<sub>3</sub> and Er,Yb:YVO<sub>4</sub> lasers near 1.6 μm for CO<sub>2</sub> LIDAR. In Proceedings of the Advanced Solid-State Photonics: Conference Paper, San-Diego, CA, USA, 31 January–3 February 2010; Optical Society of America: San-Diego, CA, USA, 2009. AMB15.
15. Ter-Gabrielyan, N.; Merkle, L.D.; Ikesue, A.; Dubinskii, M. Ultralow quantum-defect eye-safe Er:Sc<sub>2</sub>O<sub>3</sub> laser. *Opt. Lett.* **2008**, *33*, 1524–1526. [[CrossRef](#)]
16. Ma, H.J.; Jung, W.K.; Park, Y.; Kim, D.K. A novel approach of an infrared transparent Er:Y<sub>2</sub>O<sub>3</sub>–MgO nanocomposite for eye-safe laser ceramics. *J. Mater. Chem. C* **2018**, *6*, 11096–11103. [[CrossRef](#)]
17. Xue, Y.L.; Zhu, F.; Wang, J.; Sun, S.; Hu, L.; Tang, D. Fabrication and comprehensive structural and spectroscopic properties of Er:Y<sub>2</sub>O<sub>3</sub> transparent ceramics. *J. Rare Earths*. **2021**. [[CrossRef](#)]
18. Boultif, A.; Louër, D. Powder pattern indexing with the dichotomy method. *J. Appl. Crystallogr.* **2004**, *37*, 724–731. [[CrossRef](#)]
19. Yasyukevich, A.S.; Shcherbitskii, V.G.; Kisel, V.E.; Mandrik, A.V.; Kuleshov, N.V. Integral method reciprocity in the spectroscopy of laser crystals with impurity centers. *J. Appl. Spectrosc.* **2004**, *71*, 202–208. [[CrossRef](#)]
20. Repelin, Y.; Proust, C.; Husson, E.; Beny, J.M. Vibrational spectroscopy of the C-form of yttrium sesquioxide. *J. Solid State Chem.* **1995**, *118*, 163–169. [[CrossRef](#)]
21. Hou, W.; Xu, Z.; Zhao, H.; Xue, Y.; Wang, Q.; Xu, X.; Xu, J. Spectroscopic analysis of Er:Y<sub>2</sub>O<sub>3</sub> crystal at 2.7 μm mid-IR laser. *Opt. Mater.* **2020**, *107*, 110017. [[CrossRef](#)]
22. Kaminskii, A.A.; Mironov, V.S.; Kornienko, A.; Bagaev, S.N.; Boulon, G.; Brenier, A.; di Bartolo, B. New laser properties and spectroscopy of orthorhombic crystals YAlO<sub>3</sub>:Er<sup>3+</sup>. Intensity luminescence characteristics, stimulated emission, and full set of squared reduced-matrix elements  $\left| \langle \alpha [SL]J \parallel U^{(t)} \parallel \alpha' [S'L']J' \rangle \right|^2$  for Er<sup>3+</sup> Ions. *Phys. Stat. Sol.* **1995**, *151*, 231. [[CrossRef](#)]
23. Judd, B.R. Optical absorption intensities of rare-earth ions. *Phys. Rev.* **1962**, *127*, 750–761. [[CrossRef](#)]
24. Ofelt, G.S. Intensities of crystal spectra of rare-earth ions. *J. Chem. Phys.* **1962**, *37*, 511–520. [[CrossRef](#)]
25. Walsh, B.M. Advances in Spectroscopy for Lasers and Sensing. In *Judd-Ofelt Theory: Principles and Practices*; di Bartolo, B., Forte, O., Eds.; Springer: New York, NY, USA, 2006; pp. 403–433. [[CrossRef](#)]
26. Carnall, W.T.; Fields, P.R.; Wyborne, B.G. Spectral intensities of the trivalent lanthanides and actinides in solution. I. Pr<sup>3+</sup>, Nd<sup>3+</sup>, Er<sup>3+</sup>, Tm<sup>3+</sup> and Yb<sup>3+</sup>. *J. Chem. Phys. V.* **1965**, *42*, 3797. [[CrossRef](#)]
27. Gorbachenya, K.N.; Kisel, V.E.; Yasyukevich, A.S.; Maltsev, V.V.; Leonyuk, N.I.; Kuleshov, N.V. High efficient continuous-wave diode-pumped Er,Yb:GdAl<sub>3</sub>(BO<sub>3</sub>)<sub>4</sub> laser. *Opt. Lett.* **2013**, *38*, 2446–2448. [[CrossRef](#)]